



**HAL**  
open science

# PARAMETRIC DATA GENERATION OF SLAT-AIRFOIL CONFIGURATIONS USING LATTICE BOLTZMANN METHOD

Amal Roy Murali, Jérôme Boudet, Marc Jacob, Vincent Clair, Michel Roger,  
Florian Guiho, Maxime Itasse, Nicolas Molin

► **To cite this version:**

Amal Roy Murali, Jérôme Boudet, Marc Jacob, Vincent Clair, Michel Roger, et al.. PARAMETRIC DATA GENERATION OF SLAT-AIRFOIL CONFIGURATIONS USING LATTICE BOLTZMANN METHOD. 29th International Congress on Sound and Vibration, Jul 2023, Prague, Czech Republic. hal-04165654

**HAL Id: hal-04165654**

**<https://hal.science/hal-04165654>**

Submitted on 19 Jul 2023

**HAL** is a multi-disciplinary open access archive for the deposit and dissemination of scientific research documents, whether they are published or not. The documents may come from teaching and research institutions in France or abroad, or from public or private research centers.

L'archive ouverte pluridisciplinaire **HAL**, est destinée au dépôt et à la diffusion de documents scientifiques de niveau recherche, publiés ou non, émanant des établissements d'enseignement et de recherche français ou étrangers, des laboratoires publics ou privés.

# PARAMETRIC DATA GENERATION OF SLAT-AIRFOIL CONFIGURATIONS USING LATTICE BOLTZMANN METHOD

A.R. Murali, J. Boudet, M.C. Jacob, V. Clair and M. Roger

*Laboratoire de Mécanique des Fluides et d'Acoustique, University of Lyon, Ecole Centrale de Lyon, CNRS, University of Claude Bernard Lyon 1, INSA Lyon, LMFA, UMR5509, 69130, Ecully, France.*

*e-mail: amal-roy.murali@ec-lyon.fr*

F. Guiho, M. Itasse and N. Molin

*Airbus SAS, Toulouse, France*

A novel parametric data generation methodology for slat-airfoil configurations, which can aid in data-informed statistical noise modelling at low Mach numbers is developed. The methodology relies on simplified LBM simulations with a resolved near field that is coupled to a Ffowcs Williams–Hawkings (FWH) solver for far field noise predictions. The solvers are applied to a simplified slat-airfoil configuration without flap that has been developed in the EU-Project Valiant for slat noise studies and for which wind tunnel test results from ECL are available for comparison. The present methodology is first validated on the full geometry of the wind tunnel by comparing the wall pressure spectra calculations with experiments. Then a simplified uniform free flow condition is used for the parametric study. Its main advantage is to avoid expensive modelling of the original experimental setup. Two slightly modified configurations are then compared with the reference setting, one with modified slat gap and the other with a modified slat deflection angle.

Keywords: Slat noise, Lattice Boltzmann Method, Ffowcs Williams–Hawkings, Parametric Study

---

## 1. Introduction

Aeroacoustic characterisation of High-Lift Devices (HLD) in aircraft is an engineering problem regaining attention in recent years. On average, an unoptimised design of high-lift device could generate up to 10 dB of additional noise[1, 2] and is comparable to that from the landing gear. This additional noise is one among the bottlenecks towards future noise reduction targets set by major aviation authorities [3]. Hence an accurate and fast turnaround prediction tool – which can aid in parametric analysis and combined optimisation of both aerodynamics and resulting acoustics – can improve the design processes for modern aircraft. It is towards this requirement that we concoct a cost-optimised parametric simulation and inference framework for HLDs and demonstrate its applicability to the case of a standardised high-lift device. More specifically, in the present work, a Lattice Boltzmann Method (LBM) based solver *ProLB* [4] is employed for the simulation of a slat-airfoil geometry[1] with parameterisation enabled for the slat's position relative to the airfoil. The aerodynamic simulation is then coupled with a cost-efficient Ffowcs Williams–Hawkings (FWH) solver to predict the far field noise. Consideration is given to minimise the cost of each LBM simulation while obtaining the far field noise to the best accuracy, such that an extensive dataset generation is affordable. In the present paper, the choice of simulation parameters for the framework are delineated and in a future work, the resulting dataset will be utilised to enable a fast turnaround data-driven inference of noise characteristics.

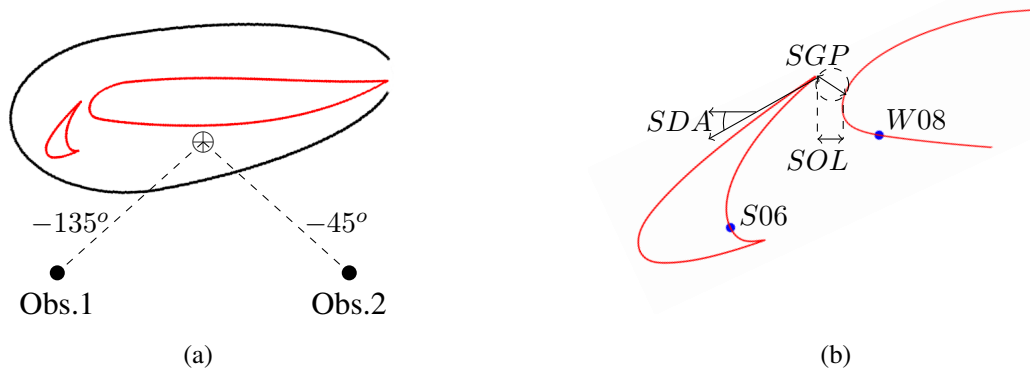


Figure 1: a) Geometry of the two element high-lift device from the VALIANT project[1], with FWL surface and relative observer positions. b) Three variable slat coordinate system relative to the airfoil and two wall pressure probes S06 and W08.

In order to enable detailed study of slat only noise using the framework, a two element design of the wing is used in the present study. The geometry was generated by Terracol et al. [1] in the EU project VALIANT by removing the flap to replace it with a sharp trailing edge and then optimizing the shape numerically such that the flow dynamics in the slat cove leading to its peculiar acoustic signature is unaffected. Moreover, the tail of the airfoil is designed to reduce the overall lift to facilitate the wind tunnel tests. A schematic of the VALIANT geometry along with FWL surface used is shown in Fig.1.

## 2. Lattice Boltzmann Method and ProLB

The Lattice Boltzmann Method (LBM) is an increasingly popular alternative to solving the Navier-Stokes equations for fluid simulations that uses a microscopic description for the fluid's behavior. On rigorous analysis the exact compressible Navier-Stokes equations can be recovered from the Boltzmann equation when correct particle collision models are assumed. Nevertheless, truncation errors of approximations for equilibrium velocity distributions in the medium often lead to discrepancies and hence fast LB schemes including ProLB are limited to isothermal and weakly compressible flows where hydrodynamic perturbations are not strong enough to produce heat sources [5], i.e. for low Mach number flows typically with  $M < 0.4$ .

LBM has specific advantages in view of aero-acoustics as well. Its implementations with variants of BGK collision models have been shown to have optimal low dissipation and low dispersion characteristics[6]. Since the numerical dissipation rates introduced are inherently less than for high order optimised schemes in Navier-Stokes solvers, the weak acoustic waves generated in low mach number flows can be efficiently propagated making LBM a prudent choice for CAA applications in aerospace industry, particularly for the airframe noise characterisation.

The ProLB solver has been specifically adapted for CAA applications as well. One such adaptation worth mention is the advancement in collision model implementation leading to the use of a Hybrid Recursive Regularised (HRR) model which makes mesh coarsening possible with minimal spurious noise generation. As shown in the work of Astoul et al.[7], the scheme is able to convect turbulent structures across refinement interfaces and avoid generation of non-physical waves, which would otherwise pollute the acoustic field due to the low dissipation nature of the solver.

### 3. Numerical test for effective dissipation and dispersion in ProLB

A classical test to quantify the effective dissipation and dispersion in the LBM solver was done using a planar Gaussian pulse. For this a one dimensional Gaussian pulse with a high pressure amplitude of 100 Pa was initialised over an otherwise quiescent initial state. ProLB was then used to advance the solution in time so as to propagate the pulse to a distance of 1m. Analysis of the pulse in the Fourier domain then allows to estimate the dissipation and dispersion effects for relevant Fourier components.

To quantitatively study the numerical dissipation and dispersion for this case, we follow the analysis by Bres et al. [8]. A reduced form of linearised Navier-Stokes equation that captures the adiabatic sound propagation in an isothermal fluid and assuming a plane wave solution leads to the dispersion relation  $(c_0^2 - i\hat{\omega}2\nu)\hat{k}^2 = \hat{\omega}^2$ . For a spatial analysis, a real frequency can be specified to obtain complex spatial wave number  $\hat{k} = \pm \frac{\omega}{\sqrt{c_0^2 - i\omega 2\nu}}$ . The phase velocity is then given by  $c_S = \omega/Re(\hat{k})$  and the spatial dissipation rate as  $\alpha_S = Im(\hat{k})$ , thereby yielding the form of a propagating 1D wave solution as

$$P'(x, t) = \hat{A} \exp(-\alpha_S x) \exp[i\omega(x/c_S - t)] \quad (1)$$

where  $c_S$  and  $\alpha_S$  are the physical phase speeds and dissipation factor for each frequency as obtained from the Navier-Stokes behavior. By including additional factors to account for numerical dissipation and dispersion in the LBM solver such that  $\alpha_s^{tot} = \alpha_s + \alpha_s^{num}$  and  $c_s^{tot} = c_s + c_s^{num}$ , and comparing Fourier transform of the above solution at different mesh locations gives their effective values as

$$\alpha_S^{num}(\omega, x) = -\frac{1}{x} \ln \left| \frac{\hat{P}'(x, \omega)}{\hat{P}'(0, \omega)} \right| - \alpha_S \quad \text{and} \quad c_s^{num}(\omega, x) = \omega x \left( \text{Arg} \left( \frac{\hat{P}'(x, \omega)}{\hat{P}'(0, \omega)} \right) \right)^{-1} - c_S \quad (4)$$

The numerical dispersion and dissipation curves obtained according to Eq.(2) for a propagation distance of 1m and for different mesh sizes are shown in Fig.2. Small negative values of  $\alpha_s^{num}$  are visible between 3 kHz and 8 kHz for  $\Delta x \geq 0.002$  m. Nevertheless, this effect does not lead to divergence in actual simulations. The total effective dissipation at 10 kHz is less than 0.01 Np/m ( $\approx 0.1$  dB/m) for a grid resolution of  $\Delta x = 0.002$  m and incur dispersion with less than 0.5% variation in phase speed. A similar resolution of 0.0016 m, obtained as a multiple of boundary layer mesh sizing of 0.0002 m, is hence chosen for the propagation of acoustic waves in the HLD simulations upto the Ffowcs Williams–Hawkings recording surface.

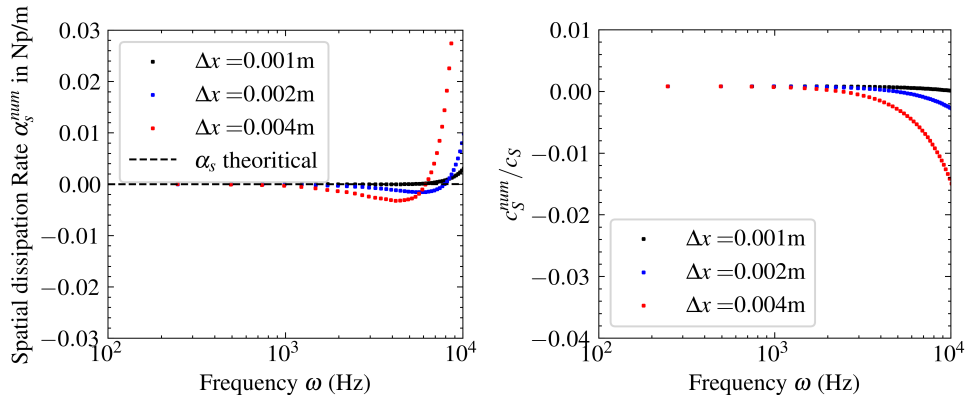


Figure 2: Left: Specific dissipation rate  $\alpha_s^{num}$  obtained for three mesh resolutions from the ratio of Fourier amplitudes for propagation distance of 1m and for frequencies up to 10 kHz. Right: Same plot for the ratio of phase speed reduction  $c_s^{num}$  with true phase speeds  $c_s$  derived from linearised Navier-Stokes.

## 4. Ffowcs Williams–Hawkings solver Turb’AcAn

A mesh size of approximately 0.002 m meets the criteria for near lossless propagation of the acoustic waves upto 10kHz. Nevertheless, the number of voxels in the Cartesian mesh used for LBM simulations scales with  $(\Delta x)^3$  and hence direct noise computation remains expensive. Here, a Ffowcs Williams–Hawkings(FWH) analogy[9] is used instead for the far-field propagation. Being an exact rearrangement of the Navier-Stokes equation in the form of a wave equation and by using the free space Green’s function to obtain an analytic integral formula for the far field sound, FWH method enables fast computation. The analogy is coded in the Turb’AcAn solver, developed at Ecole Centrale de Lyon, based on the advanced time formulation by Casalino et al.[10]. The solver has previously been tested alongside URANS[11] and LES[12] applications. In the present work, the solver is interfaced with ProLB to process the flow recordings a posteriori and simple test cases were performed which are not reported here.

Much like canonical derivation of the analogy, Casalino’s Advanced Time formulation [10] also leads to volume integrals for the quadrupole source terms causing a restriction on the placement of FWH surface. In our simulations, the surface is chosen to surround the acoustic sources in the vicinity of the airfoil and is kept far enough from the airfoil suction side to avoid strong vortices ejected from the slat cove. The surface is also open downstream of the airfoil, so that no vorticity fluctuations are convected through the surface. The integration surface used for recording unsteady data is shown in Fig.3(b) and the truncated surface used for surface integral calculation is shown in Fig.1(b). It must be mentioned that some large-size low-vorticity structures still approach the upper side of the surface but the generated spurious sound sources are negligible.

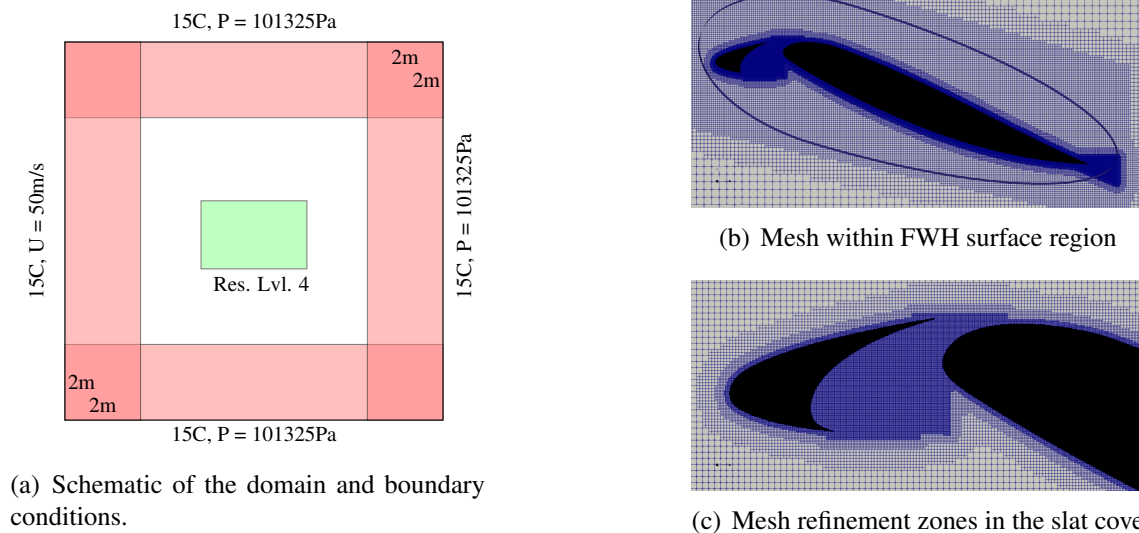


Figure 3: Template domain and mesh visualisations. The elliptical FWH surface used is shown in top right. Chord length  $C = 0.3 m$

To enable parametric LBM computations with ProLB, the pre-processing module LBPre was used to generate the meshes. A square domain with an extent of 15C, where  $C = 0.3m$  is the chord length is selected. The inflow velocity  $U = 50 m/s$  is imposed on the upstream boundary, and the static pressure  $P = 101325 Pa$  is imposed on other boundaries. In the span-wise direction, an extend of  $0.7C$  was chosen with periodic boundary conditions. A template setup consisting of the boundary conditions and refinement regions was generated first as shown in Fig.3 and the slat-airfoil geometry was defined to allow for parameter variations. Additionally, all flow boundary conditions are coupled with appropriate

absorbing boundary conditions with a region of influence of about 7C (2 m). The boundaries and applied absorbing layer settings are shown in Table 1.

Table 1: Boundary conditions applied for the simulation domain

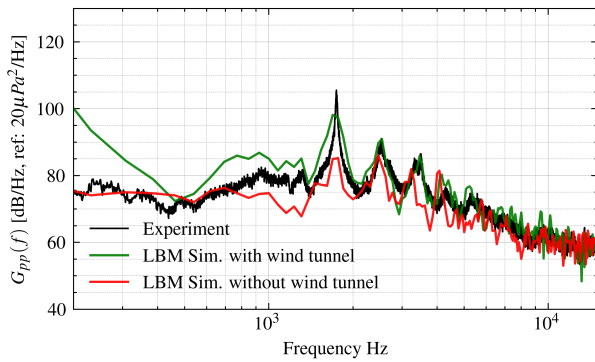
Boundary	Absorbing Layer width	Type	Mean value	Relaxation Targets
Inlet	2 m	Velocity	50 m/s	Velocity:Fixed; Pressure: Dynamic
Outlet	2 m	Pressure	101325 Pa	Velocity:Free; Pressure: Fixed
Top	2 m	Pressure	101325 Pa	Velocity:Free; Pressure: Fixed
Bottom	2 m	Pressure	101325 Pa	Velocity:Free; Pressure: Fixed
Spanwise	0 m	Periodic	None	None

To parameterise the slat’s position with respect to airfoil, a three variables coordinate system is chosen as suggested by Lu et al.[13]. The main element is kept static for all simulations. Additionally, the HRR collision model implementation in ProLB solver suffers from generation of spurious perturbations at mesh refinement interfaces while convecting vorticity[7, 14]. Additionally, as best practice with ProLB solver, the refinement interfaces are chosen, where possible, to align with coordinate axes if turbulent structures are convected across it. A uniform mesh sizing is also required inside the slat cove region to capture the aero-acoustic phenomena without spurious numerical effects. A further specification of the boundary layer element size of  $2 \times 10^{-4}$ m, corresponding to an estimated wall y-plus of 35 and uniform mesh sizing in the slat cove region leads to a mesh as shown in Fig.3(b) and 3(c). This combined with a minimisation of the mesh size leads to a discretised CFD model of airfoil is kept at  $25^\circ$  with respect to the horizontal axis.

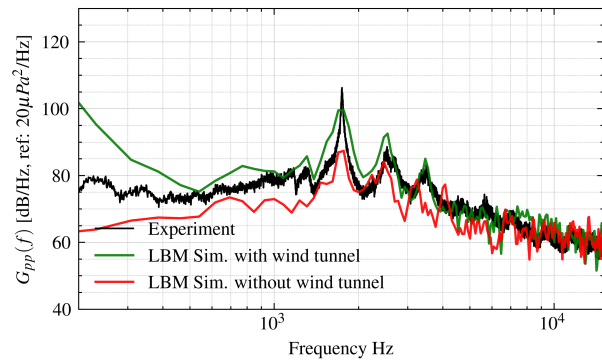
## 5. Evaluation of prototype case and parametric results

The reference case is chosen as with an angle of attack  $18^\circ$  and default coordinates for the slat position. As mentioned above, this is equivalent to the  $25^\circ$  angle of attack which was tested experimentally at ECL as part of project VALIANT[1] and the data allows to validate the reference case. The higher angle of attack used in the wind tunnel is due to the deflection of the finite width wind tunnel jet by the wing, leading to a decrease in the effective angle of attack. The correspondence between two cases was obtained empirically by Terracol et al.[1]. A key difference between the experiment and the simulation is that, in the former, end walls are present to support the mock-up. This leads to reflection of acoustic waves from the end walls and hence the possibility of span-wise standing waves. To check this effect, a separate simulation was also carried out by including the walls and numerical pressure and velocity probes corresponding to experimental measurement points were used for recording. A comparison of the wall pressure spectrum near the leading edge of the main element and inside the cove suggest that the first tonal peak (1771Hz) evident in the experiment is captured by the LBM simulation only when the set-up geometry is included. In the free flow condition where a uniform inlet velocity is specified, this tonal peak is captured with a lower SPL, suggesting a possible resonance in the wind tunnel setup. A comparison of the wall pressure spectra obtained experimentally, and LBM simulation with and without the wind tunnel geometry is as shown in Fig.4(a) and Fig.4(b). The good agreement between wind tunnel cases suggests adequate capturing of the acoustic sources by the LBM solver. The discrepancy in the first tone level and overall broadband levels between free flow and wind tunnel cases is assumed to be physical.

To validate the far field acoustic prediction capability using FWH module Turb’AcAn, the noise



(a) Probe S06 in the slat cove.



(b) Probe W08 on the main element.

Figure 4: Wall pressure spectra comparison between experimental case (—), that obtained from LBM simulation while including the wind tunnel (—), and while excluding the wind tunnel (—) for probes a)S06 and b)W08 in Fig.1(b).

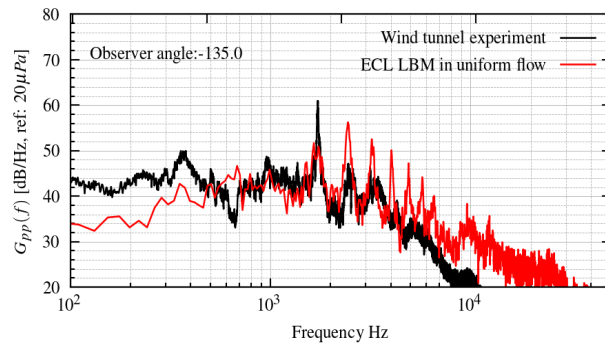
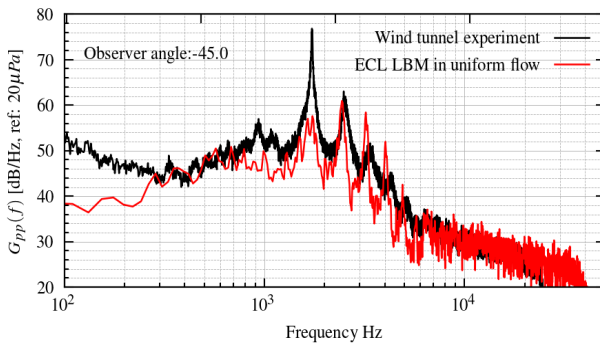


Figure 5: Comparison of far field noise spectra for observer angles  $-45^\circ$  and  $-135^\circ$  on the pressure side. Observer coordinates are with respect to the turn-table coordinate system as shown in Fig.1(b) and with radial distance of 1.8m.

spectra was computed for observers at various angles below the wing. A comparison of the result with experimental data for two observer angles  $45^\circ$  and  $135^\circ$  is shown in Fig.5. The overall shape of the numerical spectra is similar to the experimental ones. At  $-45^\circ$ , the broadband noise levels are lower than the experimental ones below 5 kHz. As expected from wall pressure spectra, the peak at 1771 Hz is also lower, but its harmonics appear more intense in the numerical results. Similar observations can be made of the peaks at  $-135^\circ$ . The results for two additional parametric cases are presented in Fig.6 and 7. These correspond to a) decrease in the slat deflection angle, and b) decrease in slat gap. For the case with a smaller slat deflection angle, the mean shear layer path followed by the vortices is increased. This can be attributed to the deviation of the shear layer path in the mean flow and correspondingly, according to Terracol's [1] formula for tone prediction, a decrease in the tonal frequencies is expected. For case b) with a decreased slat gap, the acceleration of the flow due to nozzle effect of the cove region is increased leading to a larger convection velocity of the cove vortices and hence a shift of the tones to higher frequencies. This is also in agreement with the simulation results.

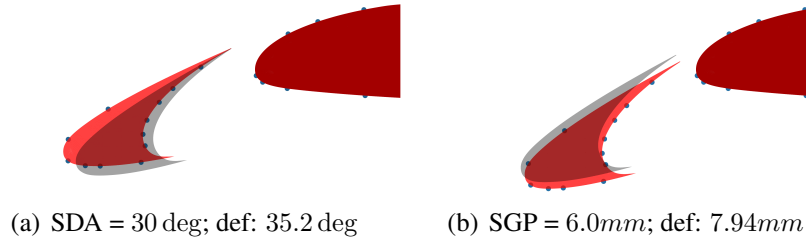


Figure 6: Slit and airfoil geometries, case a) with reduced slat deflection angle, and case b) with reduced slat gap, along with renewed wall pressure probes. Original geometry is shaded in grey.

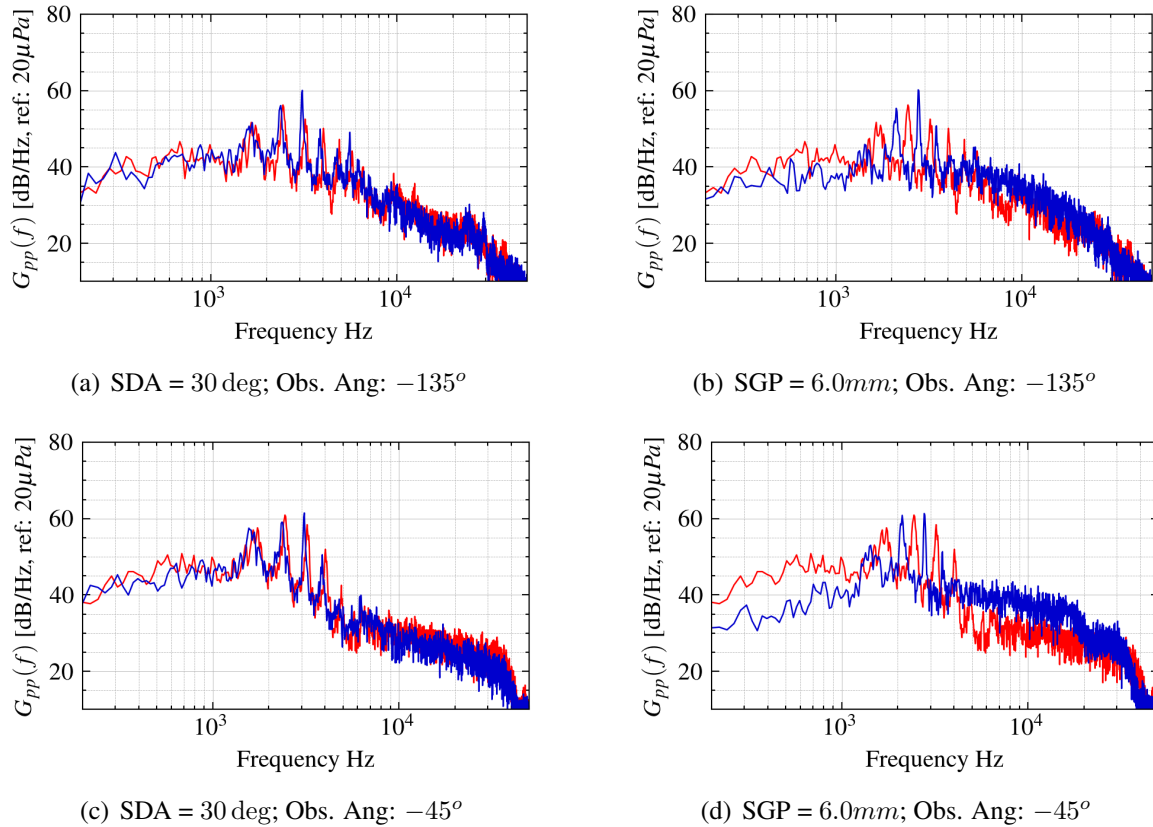


Figure 7: Spectra predictions for the two parametric cases (blue) compared against the reference case (red) and for observers Obs.1 (top) and Obs.2 (bottom) as shown in Fig.1(b).

## 6. Conclusions and future work

As demonstrated in this work, the parametric data generation framework is capable to generate acoustic predictions for slat-airfoil configurations with reasonable accuracy. This is in view of the tone frequencies and broadband noise components pertinent to slat-noise. The costs of individual simulations are minimised by employing a suitable meshing strategy along with the FWH analogy for farfield acoustic predictions. In a subsequent development of this work, a fine tuning of the FWH surface will be done to ensure suitability for parametric cases. The framework will then be employed for data generation and a fast-turnaround data-driven noise prediction strategy will be developed.

## REFERENCES

1. Terracol, M., Manoha, E. and Lemoine, B. Investigation of the unsteady flow and noise generation in a slat cove, *AIAA Journal*, **54** (2), 469–489, (2016).
2. Pascioni, K. A. and Cattafesta, L. N. Aeroacoustic measurements of leading-edge slat noise, *22nd AIAA/CEAS Aeroacoustics Conference, 2016*, (September), (2016).
3. European Commission. Directorate General for Mobility and Transport. and European Commission. Directorate-General for Research and Innovation., *Flightpath 2050 : Europe's Vision for Aviation : Maintaining Global Leadership and Serving Society's Needs*. (2011).
4. Feng, Y., Miranda-Fuentes, J., Guo, S., Jacob, J. and Sagaut, P. ProLB: A Lattice Boltzmann Solver of Large-Eddy Simulation for Atmospheric Boundary Layer Flows, *Journal of Advances in Modeling Earth Systems*, **13** (3), e2020MS002107, (2021).
5. Feng, W., He, B., Song, A., Wang, Y., Zhang, M. and Zhang, W., (2010), Compressible Lattice Boltzmann Method and Applications. Hutchison, D., et al. (Eds.), *High Performance Computing and Applications*, vol. 5938, pp. 17–26, Springer Berlin Heidelberg.
6. Marié, S., Ricot, D. and Sagaut, P. Comparison between lattice Boltzmann method and Navier–Stokes high order schemes for computational aeroacoustics, *Journal of Computational Physics*, **228** (4), 1056–1070, (2009).
7. Astoul, T., Wissocq, G., Boussuge, J. F., Sengissen, A. and Sagaut, P. Analysis and reduction of spurious noise generated at grid refinement interfaces with the lattice Boltzmann method, *Journal of Computational Physics*, **418**, 109645, (2020).
8. Brès, G. A., Pérot, F. and Freed, D. Properties of the Lattice-Boltzmann method for acoustics, *15th AIAA/CEAS Aeroacoustics Conference (30th AIAA Aeroacoustics Conference)*, (May), 11–13, (2009).
9. Williams, J. E. F. and Hawking, D. L. Sound Generation by Turbulence and Surfaces in Arbitrary Motion, *Philosophical Transactions of the Royal Society of London. Series A, Mathematical and Physical Sciences*, **264** (1151), 321–342, (1969).
10. Casalino, D. An advanced time approach for acoustic analogy predictions, *Journal of Sound and Vibration*, **261** (4), 583–612, (2003).
11. Jacob, M. C., Boudet, J., Casalino, D. and Michard, M. A rod-airfoil experiment as a benchmark for broadband noise modeling, *Theoretical and Computational Fluid Dynamics*, **19** (3), 171–196, (2005).
12. Boudet, J., Caro, J., Li, B., Jondeau, E. and Jacob, M. C. Zonal large-eddy simulation of a tip leakage flow, *International Journal of Aeroacoustics*, **15** (6-7), 646–661, (2016).
13. Lu, W., Liu, P., Guo, H. and Hu, T. Flow parameters in dominant mode selection of self-excited oscillation in slat coves, *AIAA Journal*, **59** (8), 3195–3208, (2021).
14. Astoul, T. Towards improved lattice Boltzmann aeroacoustic simulations with non-uniform grids: Application to landing gears noise prediction, (2021).